Metrology for spatial interferometry II

Yekta Gürsel

Jet Propulsion Laboratory
California Institute of Technology
800 Oak Grove Dr., Pasadena, CA 91109

ABSTRACT

Very high resolution spatial interferometry requires picometer level one dimensional metrology, surface metrology and 3 dimensional metrology. The absolute distance measurements with accuracies of only 1 part in a million are required due to the careful design of spacecraft like the proposed Stellar Interferometry Mission (SIM), carrying high resolution stellar interferometers.

An absolute calibration system for the surface gauge described in a previous paper is demonstrated.

A self calibrating absolute metrology system with a repeatability of 2 microns rms over a one way distance of a meter is demonstrated. The accuracy calibration of this gauge is in progress.

An auto aligning, 3 dimensional metrology gauge is constructed using the sub picometer linear metrology gauge described in earlier papers. Initial test results from this demonstration are presented.

1. INTRODUCTION

Very high resolution spatial interferometry requires picometer level one dimensional metrology, surface metrology and 3 dimensional metrology. The absolute distance measurements with accuracies of only 1 part in a million are required due to the careful design of spacecraft like the proposed Stellar Interferometry Mission (SIM), carrying high resolution stellar interferometers.

In three previous papers[1,2,3], a relative metrology gauge capable of sub picometer accuracy, a surface metrology gauge with sub nanometer repeatability, and initial test data for an absolute metrology gauge with an accuracy of 1 part in 10^6 were presented.

The surface metrology gauge only measured the surface figure difference between a test flat and a reference flat. In a stellar interferometer, these mirrors are the actual star tracking "siderostats". In this case, the capability of identifying the figure error of each mirror is essential for the optimal performance of the stellar interferometer.

The initial test data for the absolute gauge indicated that the laser stabilization scheme for the 1319 nm, solid state, infrared lasers is sufficient for the absolute distance measurements with the desired accuracy. Absolute measurements of the length of the frequency reference cavity were performed to an accuracy of 1 part in 10^6.

A design concept for the 3 dimensional metrology gauge was shown. Most of the needed optical and mechanical parts for this technology demonstration had been already procured.

In what follows, I will describe first the algorithm to separate the test and the reference mirror figures with the surface metrology gauge. The results of initial test runs of this algorithm are also given.

Next the test results from the completely-functional absolute metrology gauge are presented.

Finally, the completed 3 dimensional metrology gauge is presented with initial, in air test data to verify its operation. The measurements to locate the corner of a test corner cube using this 3 dimensional gauge in vacuum are in progress.

2. SURFACE METROLOGY GAUGE

2.1 Separation of Test and Reference Flat Figure Errors

A single data run of the surface metrology gauge produces a surface figure difference image between the particular test flat and the particular reference flat installed in the instrument. The surface figure error of a nearly flat mirror is defined as the deviations of its surface from the average flat surface defined by the best fitting plane to its nearly flat surface. The detailed descriptions of the surface metrology gauge and the surface figure difference algorithm are given in my previous paper [2].

In order to be able to separate the figure errors of the test and the reference mirrors, multiple runs of the gauge are required with the same pair of mirrors with at least one of the mirrors in differing positions or differing orientations. In the set of the multiple runs, no point on the moving mirror can stay fixed, as it is impossible to separate the figure errors in a small neighborhood of any fixed point.

For ease of implementation, we choose to rotate the test mirror about a single point that remains fixed through the multiple rotation runs. A different run with the test mirror slightly translated with respect to its original position is used to separate the figure errors in a small neighborhood of the center of rotation.

2.2 Deconvolution of the Center and the Angle of Rotation

Let T_f and R_f be the two dimensional surface figure errors of the particular test and the particular reference flats in a particular orientation with respect to each other respectively.

Let S_0 be the two dimensional surface figure difference error as measured by the surface gauge with the test and the reference flats in the orientation described above.

Let S_1 and S_2 be the two, 2-dimensional surface figure difference errors as measured by the surface gauge with the test mirror rotated by the angles θ_1, θ_2 around the points (x_1, y_1) and (x_2, y_2) on the surface of the test mirror from the orientation described above respectively.

Let R_1 and R_2 be the two rotation operators describing the rotations performed above.

Then, $S_0 = T_f - R_f$, $S_1 = R_1 T_f - R_f$, and $S_2 = R_2 T_f - R_f$. Define DS_1 and DS_2 as $DS_1 = S_1 - S_0$ and $DS_2 = S_2 - S_0$. It follows that $DS_1 - DS_2 = (R_1 - R_2)T_f$.

It is easy to show that $R_2 DS_1 - R_1 DS_2 = (R_1 - R_2)T_f - [R_1, R_2]T_f$ where $[R_1, R_2]$ is the commutator of the two rotation operators with different centers and different angles of rotation. I then obtain $DS_1 - DS_2 - R_2 DS_1 + R_1 DS_2 = [R_1, R_2]T_f$.

If R_1 and R_2 have a common center of rotation, then $[R_1, R_2] = 0$. This means that rotations in a plane about a common center can be performed in any order without affecting the result. In the surface metrology gauge, the test mirror rotates about a common center of rotation. This implies that

$$DS_1 - DS_2 - R_2 DS_1 + R_1 DS_2 = 0$$

The only unknowns in the equation given above are the two rotation operators with the parameters (x_0, y_0), θ_1, θ_2 that are the coordinates of the center of rotation and and the two differing angles of rotation respectively. Note that this equation holds for every pixel in the overlapping images of the surface of the mirrors. Due to the design of the surface metrology gauge [3], every pixel on the test mirror corresponds to a unique pixel on the reference mirror.

The equation given above can be expressed as $L^2 = 0$ where L^2 is a positive definite sum over all the pixels in the overlapping images of the surfaces of the mirrors. One can then minimize L^2 with respect to the parameters (x_0, y_0), θ_1, θ_2 to find the best fit values of these parameters. The only difficulty is that the images of the mirrors in the surface metrology gauge are rectangular sections defined by the imaging area of the CCD camera. Therefore, the rotated images with differing angles of rotation do not overlap entirely. A tracking minimizer with a variable region of integration dependent on the parameters of minimization is needed to handle this problem.

Figure 1: Double-differenced surface figure DS_1

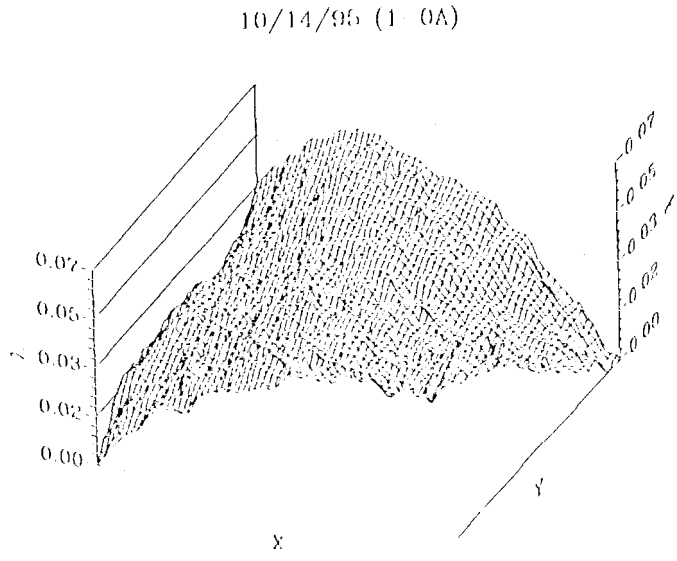

2.3. Tracking Minimizer

I implemented a variant of the Levenberg-Marquardt [4] minimization algorithm. The minimizer computes and tracks the varying region of integration as the parameters of minimization change. The returned function values to the minimizer are normalized to the area of integration to perform a meaningful minimization.

The parameters can not be allowed to change arbitrarily as the minimizer will shift the center of rotation out of the surface figure difference images with large rotation angles to get zero overlap and zero minimized value. A dynamic bound checking algorithm is linked to the minimizer to prevent it from "running out of the picture".

This method works very well and it is very fast. It takes a few minutes on a Sun Sparc 20 work station with minimal memory requirements to find the center and the two angles of rotation.

Fig. 1 and Fig. 2 show two double differenced surface figure error images (DS_1 and DS_2) with two different angles of rotation as measured by the surface metrology gauge in a particular set of data runs.

Fig. 3 shows a particular representation of the minimizer output. This is a plot of "goodness of fit" as a function of the starting coordinates of the center of rotation. The goodness of fit is zero for the absolute best fit in the absence of noise in the measurements. It is a minimum at the best-fit values of the parameters. A four dimensional minimization was performed starting from the coordinates given and the goodness of fit thus obtained was plotted at those coordinates. The initial coordinates are used instead of the final coordinates of the minimum as the minimum can be reached from many values of the starting coordinates in general.

The true rotation center appears as the dip near the center of the figure. The only other possible fits place the starting values for the center of rotation coordinates very near the edges of the figure with very bad overlap. These are eliminated by comparing them against the marked initial images of the positions of the rotating mirror.

In this particular run, the minimizer gave the values (157, 118) as the center of rotation and -0.6001 radians and 1.1878 radians as the angles of rotation. Initially, the camera was adjusted to bring the center of rotation near the center of the image at (160,120). The crudely measured angles of rotation were -0.622 radians and -1.182 radians.

Fig. 4 shows the computed center of rotation in the field of view of the camera on the derived background picture. This picture shows the imperfections in the surface gauge initial beam independent of the test and the reference mirrors. The images are compensated by this background image before the surface figure differences are computed. A new background picture is generated every time a new data run is performed to prevent any changes

Figure 2 Double-differenced surface figure DS_2

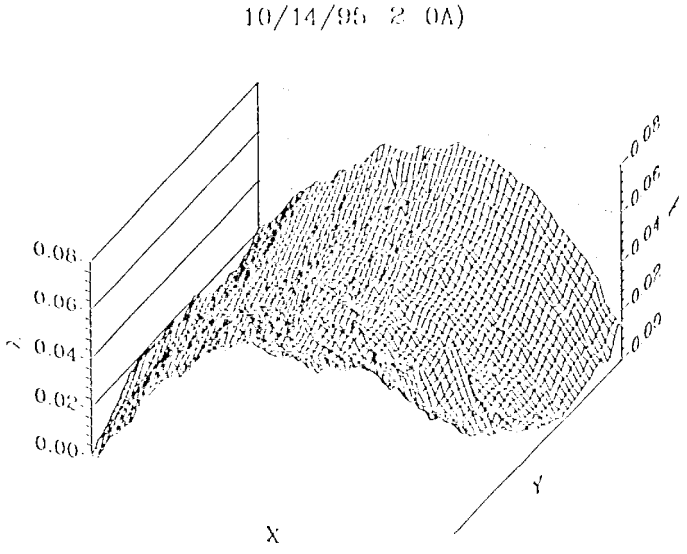

Figure 3: Goodness of fit versus the starti g center of rotation coordinates

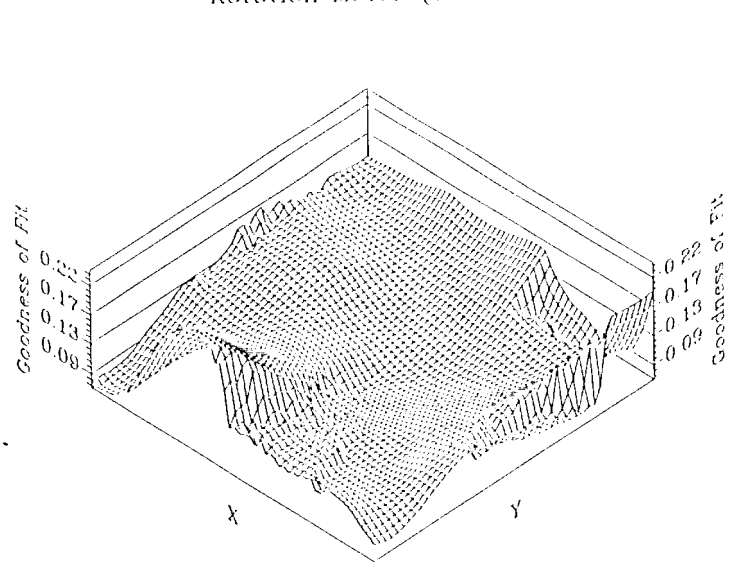

Figure 4: Computed center of rotation on the gauge background

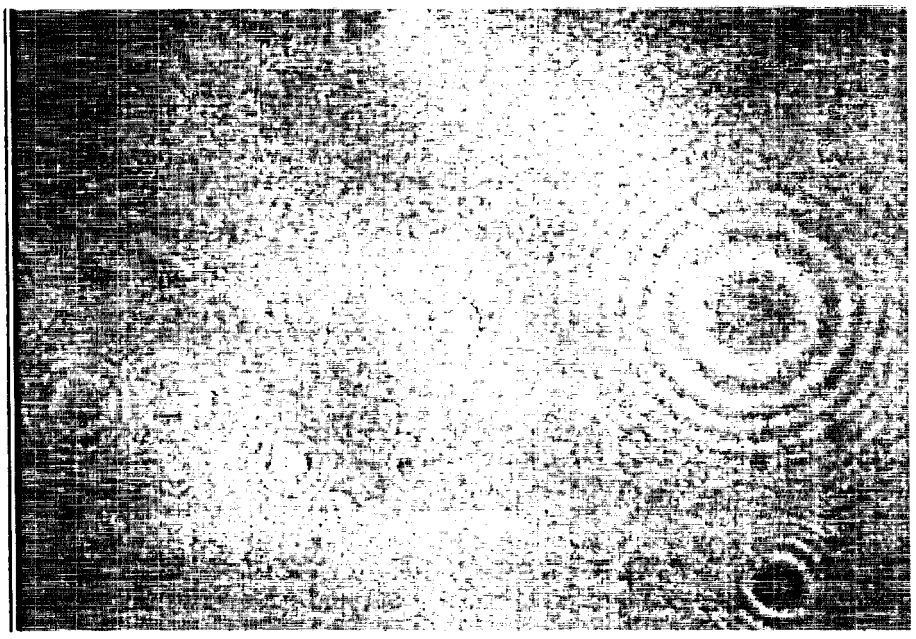

in the non-uniform background from corrupting the surface figure differences

2.4. Separation of Figure Errors

Once the the center and the angles of rotation are known, the surface figures can be solved using any pair of the equations $S_0 = T_f R_f$, $S_1 = R_1 T_f R_f$ and $S_2 = R_2 T_f R_f$. However, any straightforward attempt to [lo S[) is very likely to result in many singularities that prevent these from being used directly in a linear equation solver like Gauss Jordan elimination. One of the reasons for this is the small, singular neighborhood around the center of rotation. Another reason is the existence of closed loops in the equations due to integer pixel locations and limited precision pixel values.

In fact, these closed loops can be taken advantage of by first solving, for a small subset of points using, all three (and more using another data set) equations. The rest of the points which do not lie on a closed loop are solved for subsequently. This part of the algorithm is currently being implemented. The results of this and the translation deconvolution will be reported in a subsequent paper

3. ABSOLUTE METROLOGY GAUGE

The detailed operation of the absolute metrology gauge is described in a previous paper [3]. In what follows, I will describe the measurements performed using this gauge. Currently, the gauge operates in still air. The speed of light in vacuum is used to compute the absolute lengths. This causes a small systematic error in the lengths themselves, but it does not present a problem as the gauge repeatability is within our specifications. In space, the gauge operates in vacuum, eliminating this systematic error altogether. The demonstration will be moved into a vacuum envelope during the coming year.

3.1. Reference Cavity Length Measurements

Fig. 5 shows the optically contacted, high finesse, ULE reference cavity before it was installed in the cavity oven assembly. The vertical dark shade in the middle is produced by the small vent hole drilled into the body of the cavity. The ruler is marked in inches.

Figure 5: The reference cavity

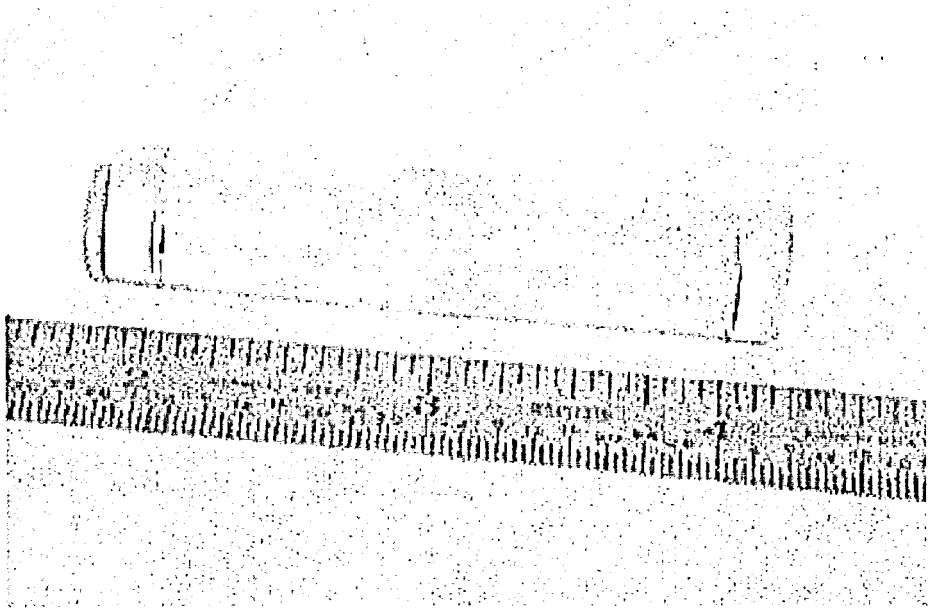

Figure 6: The cavity oven

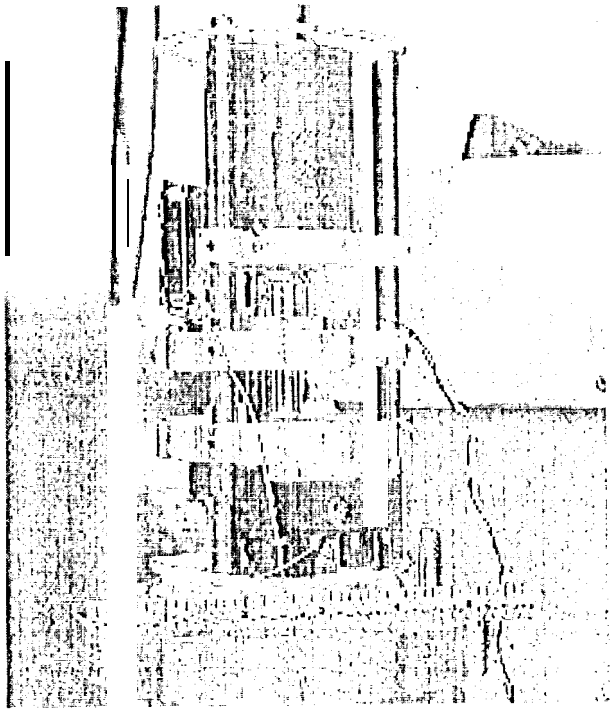

Figure 7: The reference cavity length during a day

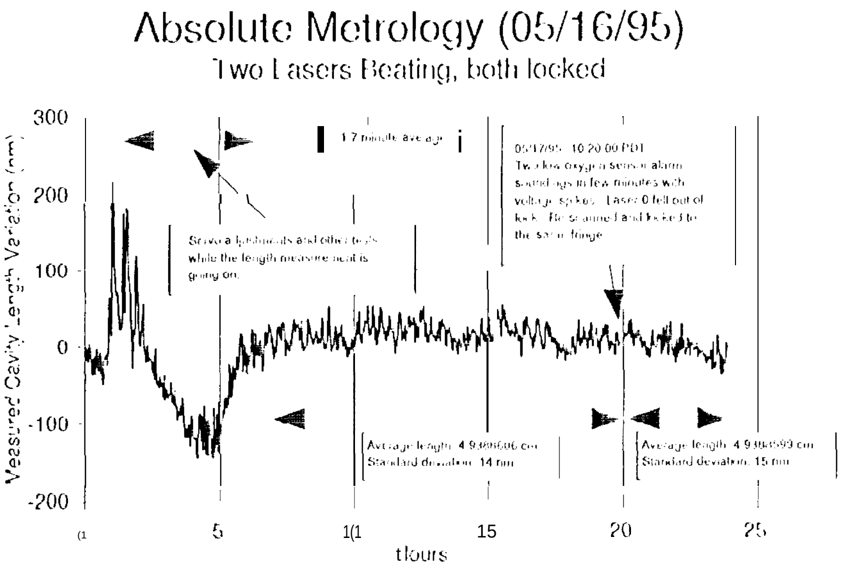

1 ig. 6 shows the cavity oven assembly with its cover removed. The cavity is suspended inside the copper canister at the top. One of the heater pads on the canister is visible. The optical circulator, the]IIO1O(l(l('(' [(11" assembly and the mode matching lens holder occupy the middle section. The bottom section houses the five axis fiber launcher assembly. A six inch ruler is resting along the edge of the 4 " inner diameter bottom conflat flange.

Fig. 7 shows measurements of the reference cavity length at every 1.7 minutes (averaging time) for a period of nearly 20 hours. The cavity length is stable to 14 nm rms.

Fig. 8 shows measurements of the reference cavity length at every 15 minutes for 120 minutes in a quieter environment. The cavity length is stable to 3 nm rms.

3.2. Simultaneous Cavity Length and Absolute Distance Measurements

Fig. 9 shows measurements of the reference cavity length for three consecutive days. The lasers were maintaining lock during this time. The cavity length is stable to 18 nm rms.

Fig. 10 shows measurements of the absolute distance for three consecutive days. The measured length was servoed to constant using another relative metrology gauge between the same corner cubes. The distance is stable 18 microns rms. The actual distance measured was verified with a ruler to an accuracy of few millimeters.

Fig. 11 shows measurements of the absolute distance one after another with improved laser stabilization and absolute gauge code. The measured length was held constant using another relative metrology gauge between the same corner cubes. The distance measurement is repeatable to 2 microns rms.

New data indicate a repeatability down to 1 micron rms over the same absolute distance. These results together with a calibration tracking run (changing distance tracked by the absolute gauge) and absolute gauge vacuum results will be reported in a subsequent paper.

4. 3-D METROLOGY GAUGE

The completed 3 dimensional metrology gauge is presented in the figures Fig. 12, Fig. 13, and Fig. 14. Five linear metrology heads with built in dithering are mounted on a 2' by 2' super invar breadboard. These heads monitor the distance between their internal corner cubes and one external corner cube. The external corner cube is mounted

Figure 8: The reference cavity length for two hours

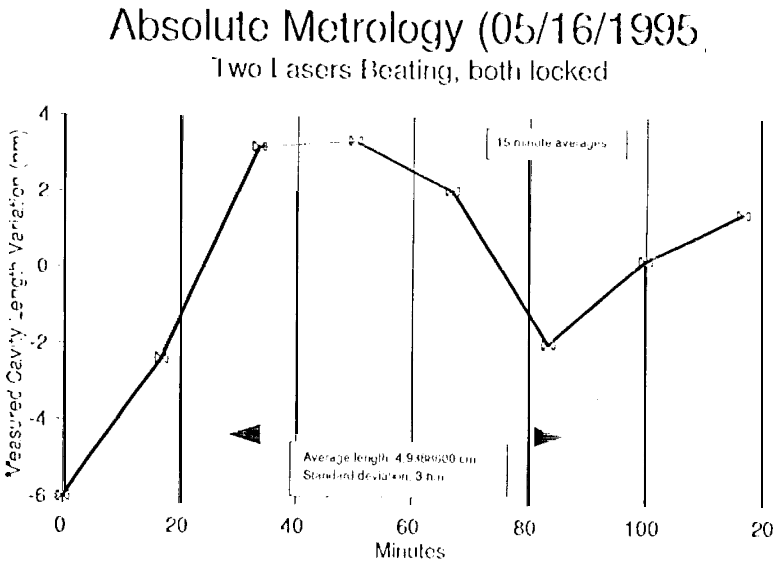

Figure 9: The reference cavity length for three days

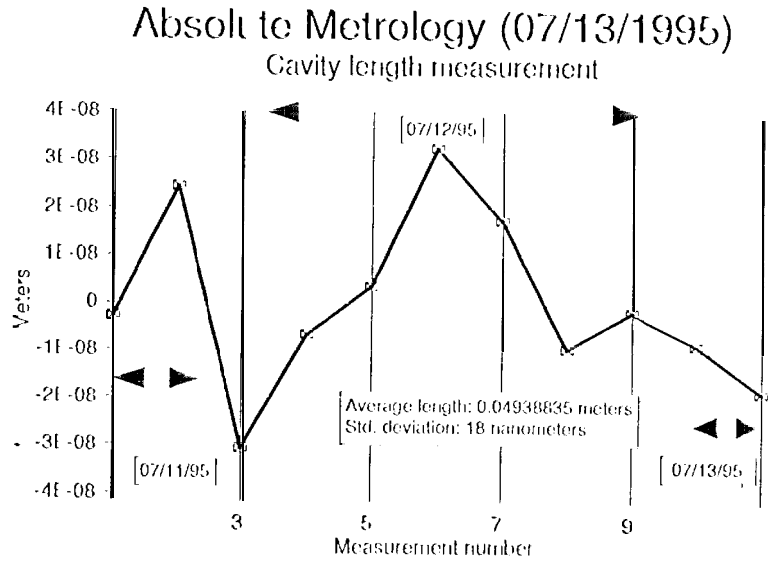

Figure 10: The absolute distance for three days

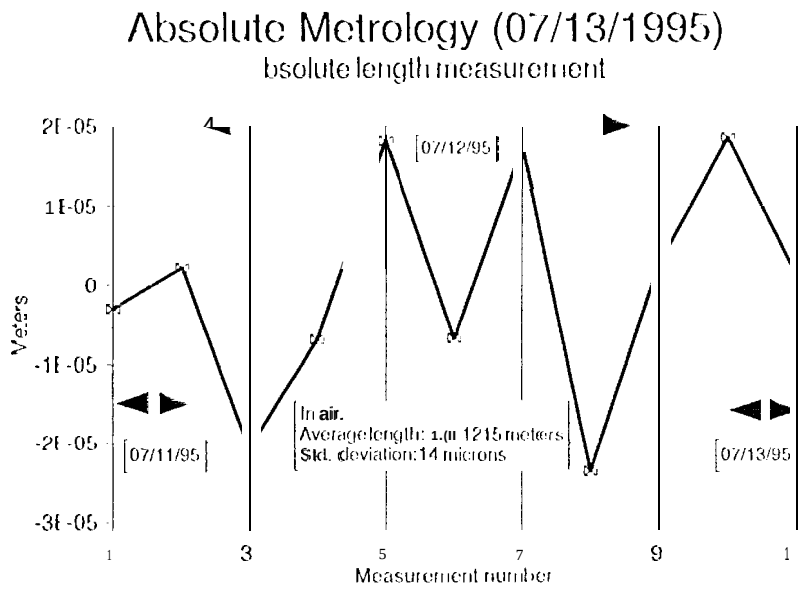

Figure 11: Improved repeatability

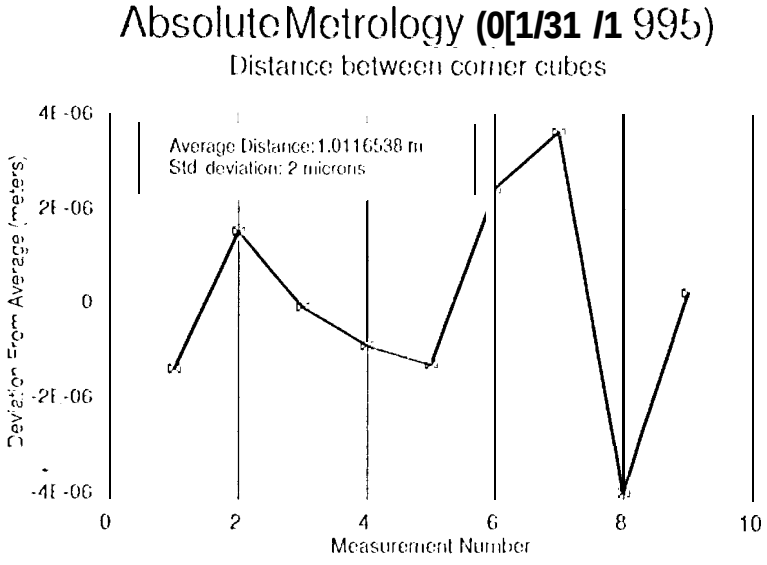

Figure 12: The 3-D metrology configuration

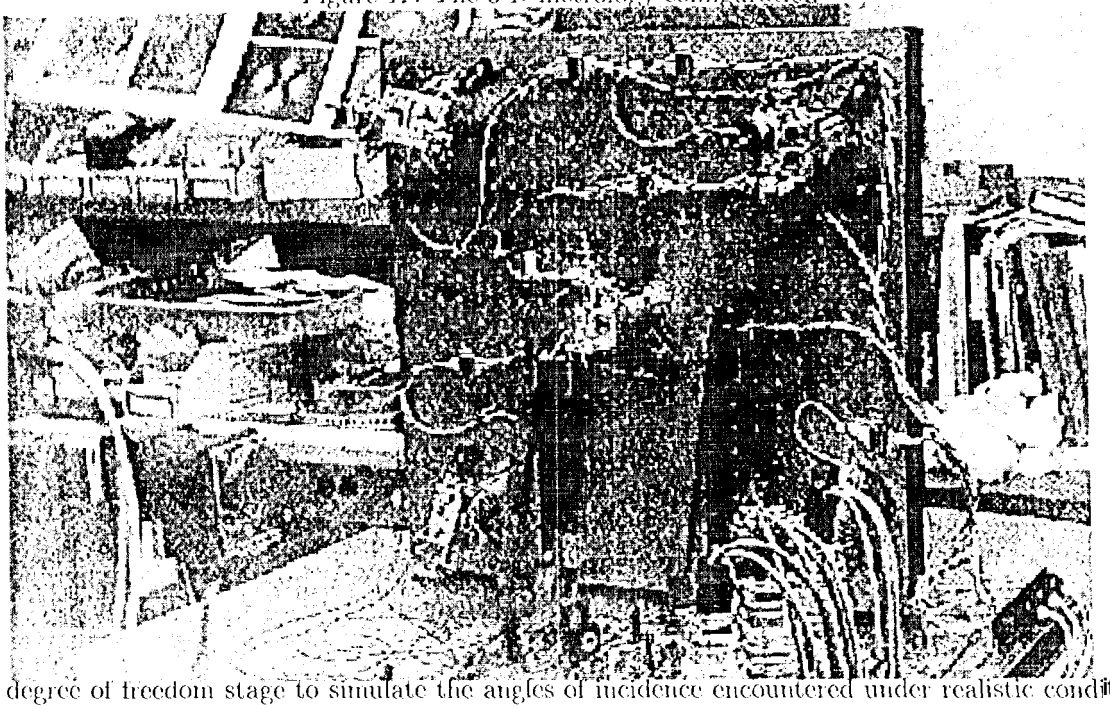

on a five degree of freedom stage to simulate the angles of incidence encountered under realistic conditions. The breadboard acts as a thermally stable reference surface that holds the distances between the measurement heads constant.

The design uses the previously developed [1,2], linear relative metrology gauge. The improvements to the linear gauge include an all-fiber distribution system and built-in dithering on a thermally stable base. The modulation system is the same as the one used in the absolute metrology gauge. The entire gauge once again is constructed on a seismically isolated optical breadboard inside the four feet vacuum chamber.

The gauge is driven by one of the stabilized lasers that also functions in the absolute gauge. The fibers bring the heterodyne beams to the 3-dimensional gauge base table. A 2 by 5 fiber splitter generates all the laser beams needed for the five heads.

The metrology launching head consists of two fiber collimators, a polarizing beam combiner, a beam launcher cube, a reference corner cube, reference and unknown photodetector circuits and the dithering, piezo-electric tip-tilt stage. Five heads are arranged in such a way that all of their beams intersect at the corner of the measurement corner cube.

The measurement corner cube is mounted on a piezo-electric flexure mount approximately 33 inches away from the super invar table. This mount is used to hold the distance between the central head and the measurement cornercube constant. It is also used to change this distance predictably and accurately.

The initial tests of the system consist of measuring the ('10S('(1 loop performance of the measurement corner cube servo system and determining the tracking error between any pair of heads in air, without seismic isolation) air current dampers or self-interference cancellation to get a baseline set of data before moving it into the vacuum envelope.

Fig. 15 shows one second averages of the servo error signal of the measurement corner cube servo system under the conditions described above. The residual jitter is about 39 pm rms. The unity gain oscillation frequency of this servo is 444 Hz. The servo error signal is sampled at 4096 Hz, and feedback is applied through a simple integrator.

Fig. 16 shows the tracking error between two heads when the measurement corner cube is moved in a rapid cycle to cancel out the effects of air turbulence and ground vibrations. The servo is made to oscillate at its unity gain frequency. The peak-to-peak amplitudes of the motions detected at each head at every half cycle of the oscillation is compared to each other. The ratio of these peak-to peak amplitudes is constant and it is a function of the angle

Figure 3 The 3-D metrology launching head

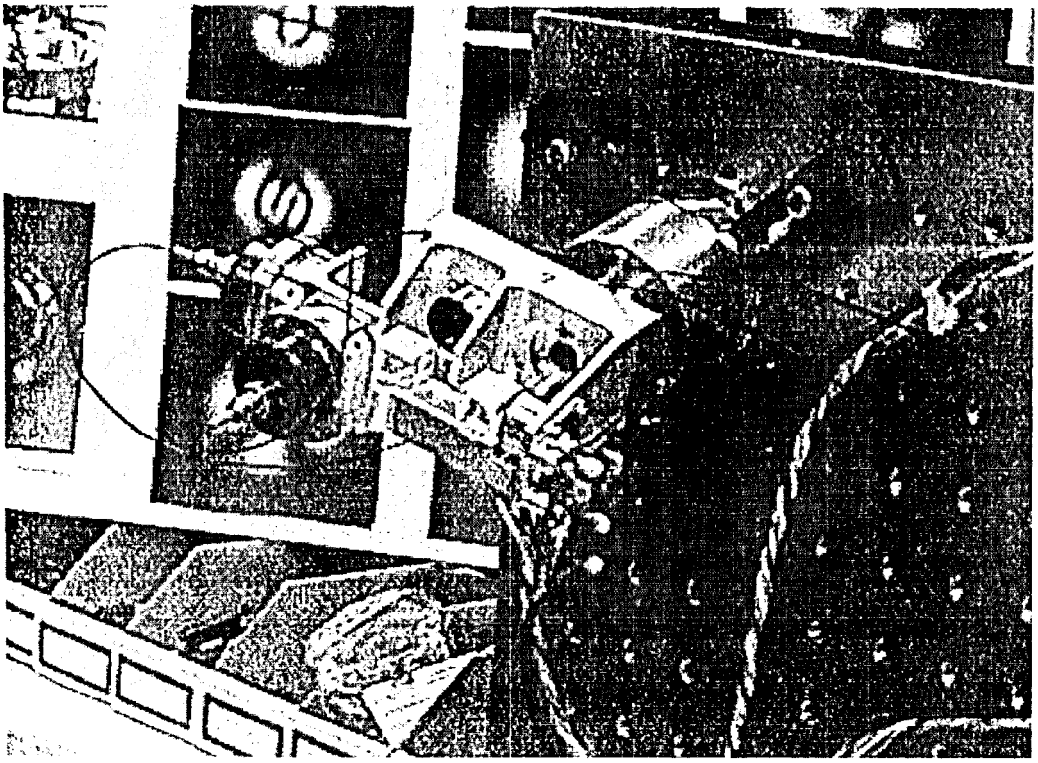

Figure 14: The 3-D metrology measurement corner cube

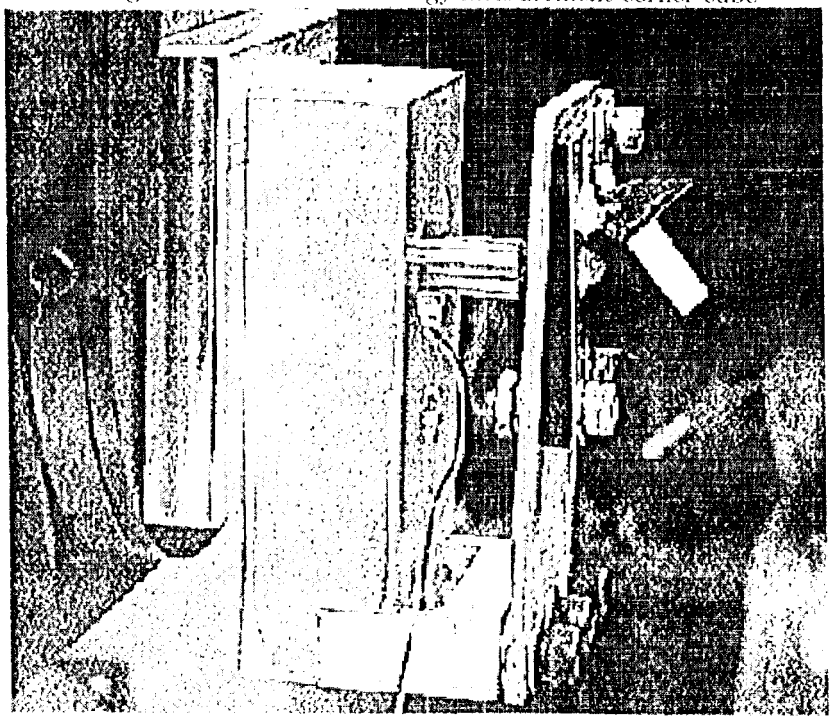

Figure 15: The 3-dimensional gauge servo error signal

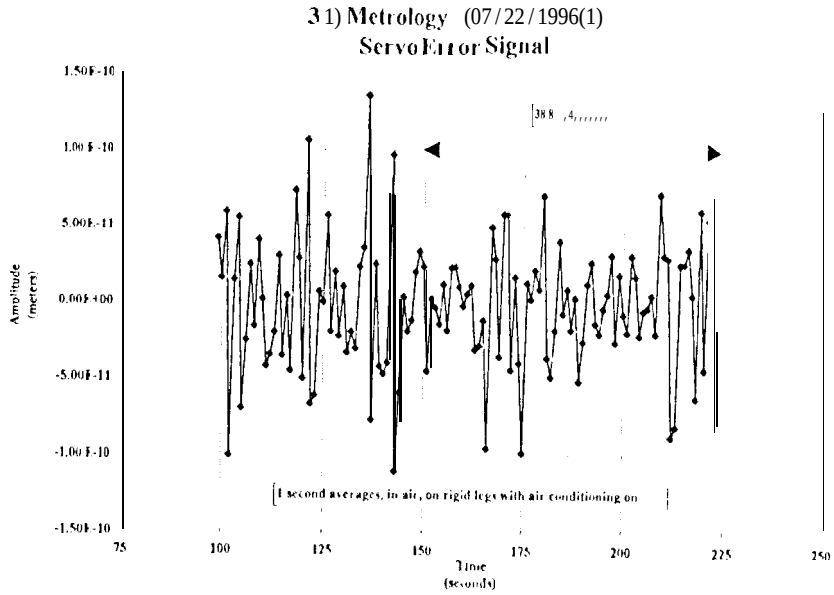

Figure 16: Tracking error between two heads

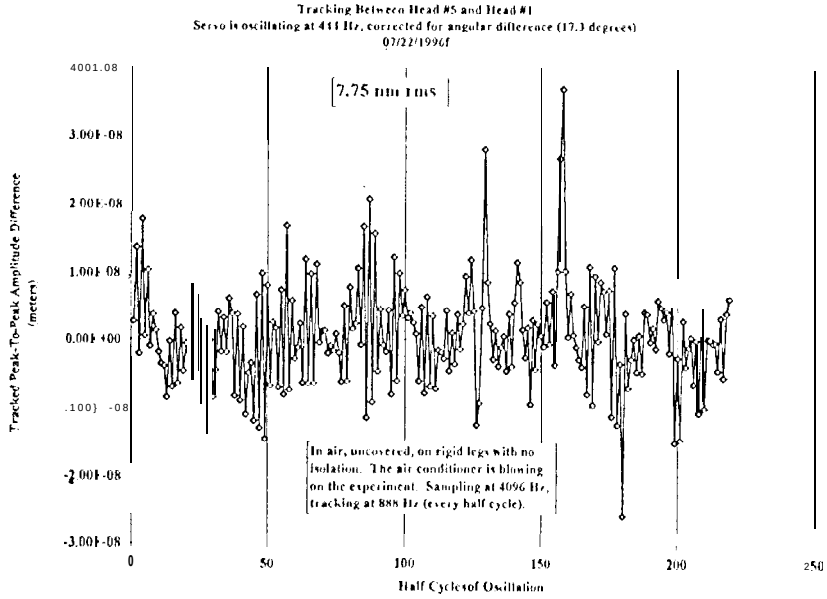

Figure 17: The input beam to a corner cube

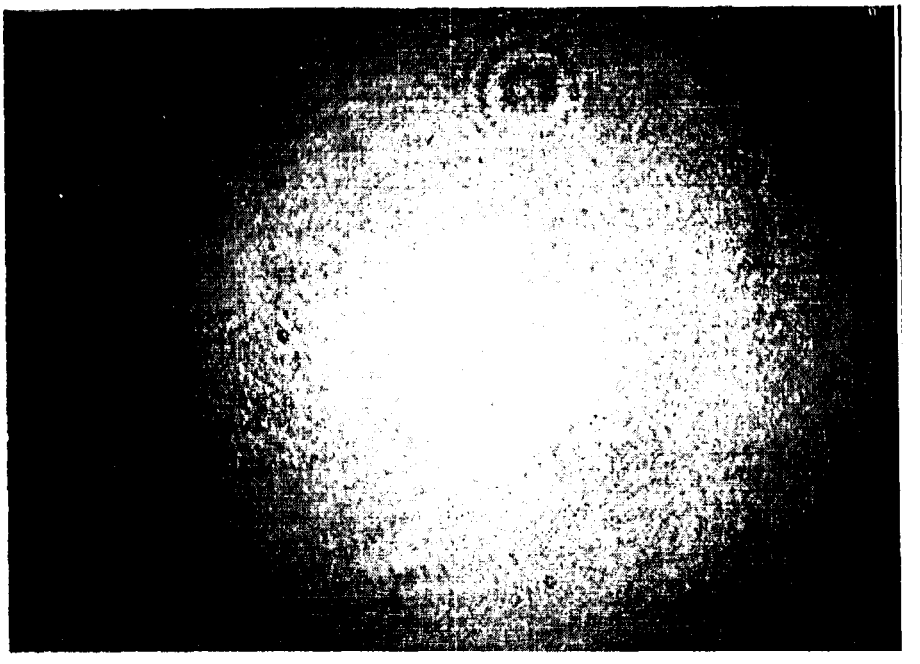

between the heads. This particular data set indicated an angle of 17.3 degrees ± 1 degree between these two heads. A crude measurement using a ruler gave an approximate angle of 20 degrees with an error of ± 2 degrees between the same heads. The difference between the motions detected at these heads after accounting for the derived angle difference is about 8 nm rms.

4.1. Corner cube induced aberrations

Fig. 17 shows a 10 mm visual diameter, nearly Gaussian laser beam with a wavelength of 633 nm impinging on a 2" clear aperture, few' arc-second orthogonality, $\lambda/10$ each surface figure, open-faced corner cube.

Fig. 18 shows the returned beam from the same corner cube nearly 1.5 meters away. The beam looks like anything but a Gaussian. In the 3-dimensional metrology gauge, an output beam, after being reflected by two corner cubes, is made to interfere with a beam that looks like the input beam as show II in Fig. 17. When the input beam moves to dither, the deep diffraction pattern moves with it potentially causing large phase errors. The 3 dimensional gauge will solve for and eliminate these types of systematic problems as well.

The in-vacuum results from this gauge with dithering, will be reported in the subsequent paper.

5. SUMMARY

The surface gauge absolute calibration is in progress. The deconvolution of the rotation from the surface figure difference images is complete. The solution for the separated surface figures is being implemented. These results and the translation deconvolution will be reported in a subsequent paper.

The absolute gauge has reached a cavity length measurement accuracy of 3 nm rms for a cavity length of nearly 5 cm. The absolute distance repeatability is down to 2 microns rms for a one-way distance of nearly 1 meter. New data indicate down to 1 micron repeatability in air. The calibration of this gauge by tracking a changing distance and the gauge operation in vacuum will be reported in the subsequent paper.

The construction of the 3-dimensional metrology gauge is complete. The gauge is being tested in air before it is placed in vacuum. The results from this gauge will be presented in the subsequent paper.

Figure 18: The output beam from the same corner cube

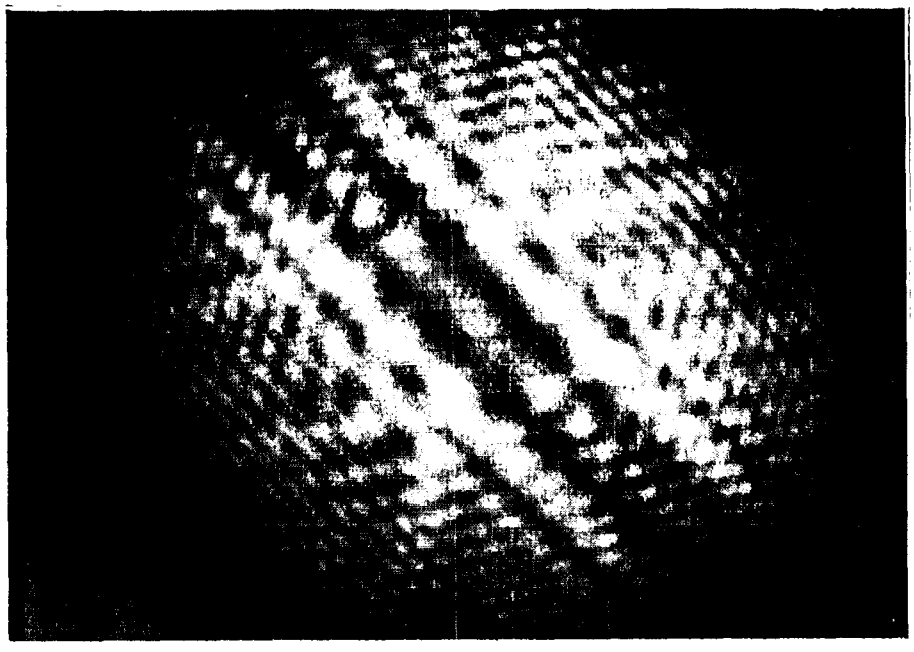

6. ACKNOWLEDGEMENTS

I would like to thank M. Shao and J. Yu for many fruitful discussions. I would also like to thank D. Moore for his design of the mechanical structure of gauge heads. The research described was performed at the Jet Propulsion Laboratory, California Institute of Technology, under a contract with the National Aeronautics and Space Administration.

7. REFERENCES

1. Y. Gürsel. Laser metrology gauges for OSI, *in Proceedings of SPIE conference on Spaceborne Interferometry*, vol. 1947, p. **188-197,1993.**

2. Y. Gürsel. Metrology for spatial interferometry, *in Proceedings of SPIE conference on Amplitude and Intensity Spatial Interferometry*, Vol. 2200, p. 27-34, 1994.

3. Y. Gürsel. Metrology for spatial interferometry II, *in Proceedings of SPIE conference on Spaceborne Interferometry II*, Vol. 2477, p. **2?40-258,** 1995.

4. William H. Press, Brian P. Flannery, Saul A. Teukolsky and William T. Wetterling, NUMERICAL RECIPES, The Art of Scientific Computing, Sections 14.3-14.4, Cambridge University Press, 1986.